Characterization of Hard Metal Dusts from Sintering and Detonation Coating Processes and Comparative Hydroxyl Radical Production

Michael J. Keane,*,† Jennifer L. Hornsby-Myers,† James W. Stephens, Joel C. Harrison,† John R. Myers,‡ and William E. Wallace†

Health Effects Laboratory Division, National Institute for Occupational Safety and Health, 1095 Willowdale Road, Morgantown, West Virginia 26505, and Division of Safety Research, National Institute for Occupational Safety and Health, 1095 Willowdale Road, Morgantown, West Virginia 26505

Received April 2, 2001

Dust samples from sintering and detonation coating hard-metal processes were characterized, compared, and contrasted for morphology, composition, and generation of hydroxyl radicals. Inhalation of respirable hard-metal (sintered carbide) dusts from hard-metal processes is known to cause fibrotic and asthmatic lung disease. Scanning electron microscopy/energy-dispersive X-ray analysis was used for morphology, composition, and elemental distribution. An electron spin resonance (ESR) spin trapping technique was used to detect hydroxyl radical generation. Samples were incubated with air-saturated buffer solutions containing a spin trap and analyzed by ESR for the presence of •OH in solution. Postdetonation coating samples often had surface contamination of Co on the WC particles, as shown by elemental mapping of individual particles; this was not evident in predetonation samples or unsintered materials in this study. ESR measurements show that both detonation-gun materials were capable of generating •OH, while the WC, cobalt, and presintered mixture did not produce detectable amounts of •OH radicals. The DMPO/•OH adduct formation was apparently facilitated by Fe-mediated reactions for predetonation dusts, and by Fe-mediated site-specific reactions for postdetonation dusts. The overspray materials from the detonation-gun process produced 9-fold more •OH radicals than the predetonation coating mixture. Overall, this study indicates there are substantial differences between postdetonation materials and both predetonation and unsintered hard-metal process materials with respect to morphology, elemental distribution, and •OH radical generation reactions and that these differences may be important in the toxic potential of those materials.

Introduction

Hard metals are composites consisting of metallic carbides, usually tungsten carbide (WC), with a metallic binder, generally elemental cobalt. Cobalt content generally ranges from 5 to 15%, while the tungsten carbide content generally exceeds 80% (*1*). Some formulations also contain carbides of Ti, Ta, V, Cr, Nb, and possibly other transition metals. Typical industrial applications are for drilling bits, cutting edges for tools and saw blades, and dies for metal forming. NIOSH estimated in 1977 that over 30 000 individuals are exposed to hard-metal dusts at industrial worksites (*2*).

Several pulmonary diseases have been linked to hard-metal dust exposure: asthma (*1*, *3*−*6*), pulmonary fibrosis (*1*), and lung cancers (*7*). Asthmatic disease is believed to be linked to the cobalt content (*1*). Hard metal exposure has been long linked to lung fibrosis (*8*−*10*). A typical disease pattern is characterized by diffuse interstitial fibrosis with large mononuclear and occasional multinucleated giant cells. Occupational exposures are generally monitored by measuring workplace area and personal exposure to cobalt; the NIOSH recommended exposure limit (REL) for Co is 50 μg/m^3 and the OSHA permissible exposure limit (PEL) is 100 μg/m^3. Hard metal exposures have also been linked to excess lung cancers in the French hard-metal industry workers (*7*). IARC (*11*) has classified cobalt and cobalt compounds as possible human carcinogens (Group 2B).

A case study in a hard-metal coating facility (*12*, *13*) has generated some concern; a process for coating parts with hard-metal materials has generated adverse health effects despite the fact that Co exposures were in compliance with the PEL. One case at a detonation coating plant identified hard-metal disease in a worker with less than 10 years exposure and a fatality in a supervisor (*12*, *13*); hard-metal exposures of those individuals, however, were not exclusively from detonation coating processes and may have included hard-metal exposures from high-velocity oxy-fuel and plasma spraying.

The objectives of this study are to physically and chemically characterize materials from both sintering and detonation coating processes and compare the results

* To whom correspondence should be addressed.
† Health Effects Laboratory Division.
‡ Division of Safety Research.

[1] Abbreviations: BET, Brunauer−Emmet−Teller; DETAPAC, diethyltriaminepentaacetic acid; DMPO, dimethyl-1-pyrroline *N*-oxide; DMSO, dimethyl sulfoxide; EDS, energy-dispersive X-ray analysis; IARC, International Agency for Research on Cancer; PEL permissable exposure limit; ROS, reactive oxygen species; REL, recommended exposure limit; SEM, scanning electron microscopy; SOD, superoxide dismutase; XRF, X-ray fluorescence spectroscopy; ZAF, Z(atomic number)-absorption-fluorescence correction method for EDS analysis.

10.1021/tx0100688
Published on Web 06/22/2002

to pinpoint what variables may be critical in hazard potential. The hypothesis to be tested is that the detonation process material has distinct physical and chemical characteristics attained during the process, possibly related to the generation of reactive oxygen species, relative to the materials from sintering processes.

Materials and Methods

Two hard-metal samples were obtained at a detonation coating facility: a sample of the process feedstock ("predetonation" material) and a sample of the overspray ("postdetonation") material. The detonation coating process involves the charging of both a powder mixture and an air−acetylene mixture to a gun-type apparatus and igniting the charge, which heats and propels the powder components onto the target part to be coated. The barrel is purged with N_2, and the process repeated several times per second. Temperatures are sufficiently high to melt many metallic materials; overspray material that misses the target may fuse with other debris in the coating booth. Overspray materials may also include dusts from other coating processes besides hard-metal coatings. WC and Co samples were the materials used in formulating sintered hard-metal products. The unsintered sample was the blended WC−Co mixture before molding and sintering. All materials were stored at room temperature in sealed containers until use.

Specific surface-area determinations were made with a pressure-flow BET instrument (Micromeritics, Norcross, GA.), using purified N_2 as the adsorbate and He for freespace determination. Approximately 5 g of materials was weighed into tubes and conditioned for 1 h at 200 °C under N_2 and capped, cooled, and reweighed. N_2 adsorption isotherms were determined using a five-point algorithm; triplicate measurements were made for each sample.

Particle size determinations were done using a TSI (St. Paul, MN) aerodynamic particle sizer, which has an effective range of 0.5−20 μm. Scanning electron microscopy (SEM; JEOL model JSM 6400) identified some additional particles smaller than 0.5 μm. SEM was also used to record high-magnification images of particles and particle clusters, and for discrete particle elemental composition and elemental maps on the aggregates, using energy-dispersive X-ray spectroscopy (EDS) (Princeton Gamma-Tech, Princeton, NJ). Samples were prepared for SEM analysis by weighing ~1 mg of material into a glass tube, adding 10 mL of 2-propanol, sonicating 10 min at 55 W, and pipetting 10 μL of suspension onto a polished carbon stub. Images were taken at 19 mm working distance, an acceleration potential of 20 keV, and a detector takeoff angle of 26°. Magnification was 1000, and the conditions allowed any object of 0.5 μm or greater diameter to be identified and measured. To ensure that sufficient numbers of fields of particles were examined to be representative of the entire SEM stub, the minimum field number was calculated as

$$n = s^2/(0.1E)^2 \quad (1)$$

where n is the number of necessary fields, s is standard deviation, E is the mean, and 0.1 is the desired relative standard error (i.e., 10% sampling error). The statistical power of this sample was set at 65%. Means and standard deviations are calculated from the total areas of all objects in each field, from a total of 10 or more fields.

Discrete particle composition analyses were made by SEM-EDS as described above, in several steps.

(1) Objects were identified and labeled in each field.

(2) A 60 s live-time EDS spectrum was acquired for each object, and all elements were identified by characteristic energies.

(3) Spectra were overlaid in blocks of 20 to positively establish the elements present. Overlapping lines and interferences were resolved by examining higher order line patterns, and nonparticle objects, such as stub defects, were eliminated. A list of all elements present in the sample was generated.

(4) Quantitative results for the list of elements were computed and tabulated, using ZAF correction algorithms, normalizing the results to a total of 100 wt % (after excluding elements lighter than Na).

(5) Normalized elemental composition results were plotted on ternary (triangle) diagrams for three selected components or sums of components. Typically for the hard-metal samples of this study, W and Co were selected for two of the axes, and the sum of all other elements found was plotted on the third axis. Diagrams may then be examined for clusters of similar particles; data points in a cluster can be isolated and replotted using different axis assignments. In this way, patterns of composition may be examined for large numbers of particles in a sample, and the compositional spectrum of a sample determined. Quantitative results from EDS using the ZAF approximations need to be interpreted with some degree of caution but are used here for classification purposes, rather than analytical procedures of high accuracy and precision. Bulk chemical analysis was done by X-ray fluorescence (XRF) analysis through the NIOSH Division of Applied Research and Technology, Cincinnati, OH. A Bruker wavelength-dispersive XRF spectrometer was used to quantitate W, C, Co, Cr, V, Ni, Ti, Ta, and Nb.

ESR spectroscopy was used to measure hydroxyl radical (•OH) production by hard-metal materials in solution. Fifty milligrams of each material was weighed into vials, and 900 μL of air-saturated phosphate-buffered saline (PBS, Gibco, pH 7.4) was added, as well as 100 μL of 0.5 M dimethyl-1-pyrroline *N*-oxide (DMPO, Sigma-Aldrich) in 18.2 MΩ cm H_2O. DMPO was purified before use with ultrafine charcoal. The mixture was left to stand for times of 10,15, 30, 45, and 60 min, and the liquids were removed with a syringe, filtered through a 0.2 μm syringe filter, the liquid added to a flat ESR sample tube (Wilmad, Buena NJ) with a 0.1 mm path length and inserted into a Varian E-109 spectrometer. The spectrometer settings were RF frequency, 9.45 GHz; center field, 3365 G; RF power, 25 mW; and modulation amplitude, 0.5 G. The negative control was PBS + DMPO only. Twenty five milliwatts of power and a receiver gain of 8000 were in the linear portions of response curves for the spectra with strongest intensity. Hydroxyl radical relative concentrations were estimated from peak areas calculated as the product of one-half of the peak height and the peak-to-peak width squared, measured in millimeters from the (derivative) spectra. To rule out DMPO/•OH adducts from degradation of DMPO adducts of superoxides and other species, sodium formate was added to selected samples to final concentrations of 25, 50, and 100 mM, to react competitively with •OH radicals. Oxygen consumption was examined using the Gilson Oxygraph polarographic analyzer. Metal-ion chelators, deferoxamine, diethyltriaminepentaacetic acid (DETAPAC), and 1,10-phenanthroline (Sigma-Aldrich) were added to final concentrations of 0.5, 0.5, and 5 mM, respectively, to determine whether metal ions in general and Fe ions in particular have an influence on radical generation. Catalase (2000 units/mL, Sigma-Aldrich) and superoxide dismutase (5 μg/mL, Sigma-Aldrich) were used to examine the involvement of hydrogen peroxide or superoxide in •OH radical generation. Oxygen-free experiments were done in a glovebag with all solutions, containers, and apparatus purged at least 15 min with N_2. Hard-metal samples were treated for 60 min at 200° C under N_2. Metal concentrations in filtered solutions from the ESR time study were measured for Co, Fe, Ni, and Cr at 10, 15, 30, 45, and 60 min for unsintered, predetonation, and postdetonation materials by inductively coupled plasma-atomic emission spectroscopy through the NIOSH Division of Applied Research and Technology. Powdered Fe (<2 μm), Cr (<10 μm), and Cr_3C_2 (−325 mesh) (Alfa-Aesar, Ward Hill, MA) were added to unsintered material in proportions equivalent to that found in the post-detonation coating materials, and assayed for •OH radical generation as described above. Amounts in samples were 49.8 mg of unsintered + 0.2 mg of Fe; 49 mg of unsintered + 0.95 mg of Cr, and 48.9 mg of unsintered + 1.1 mg of Cr_3C_2, respectively. Unsin-

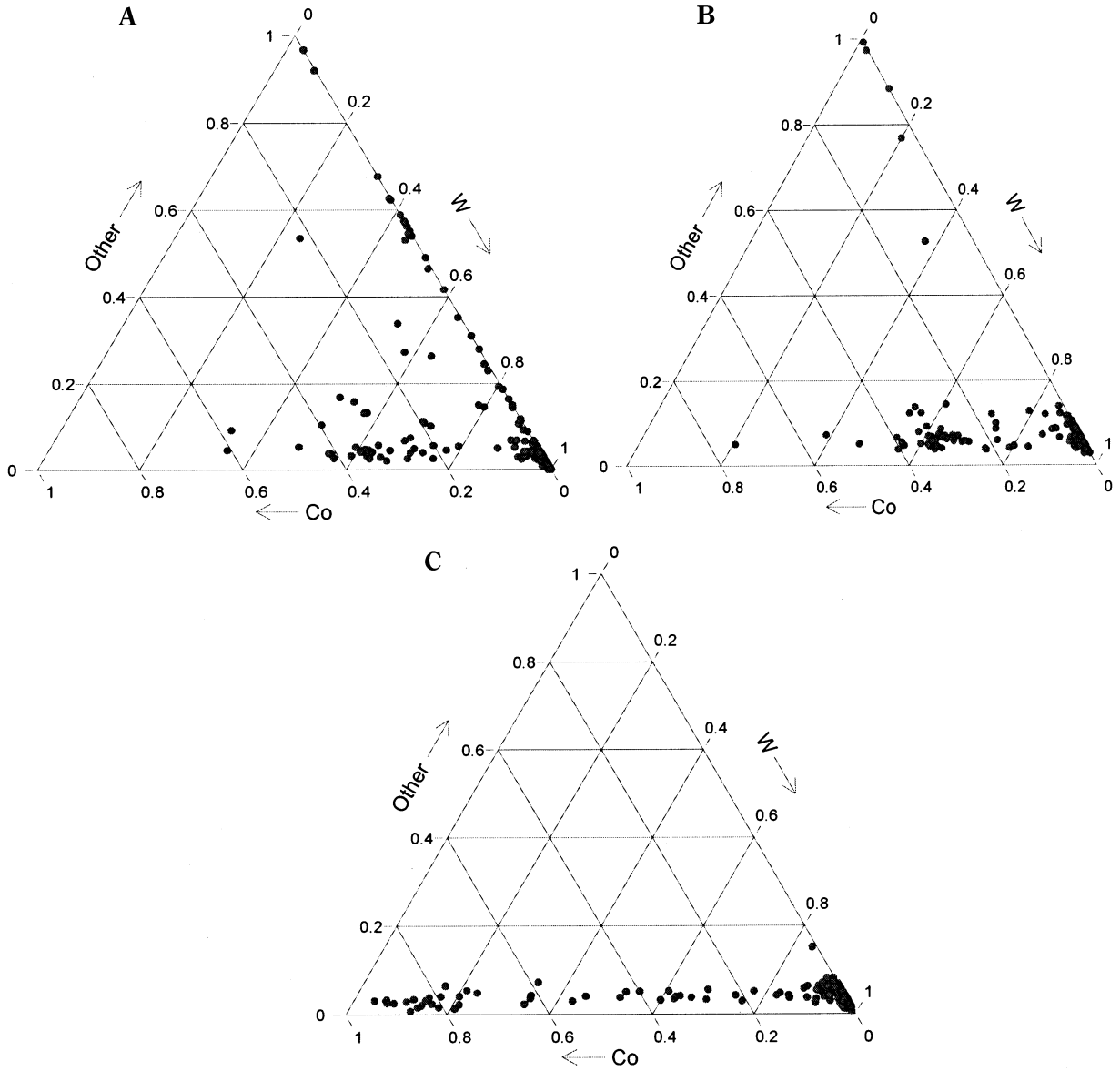

Figure 1. Ternary elemental composition diagrams for hard-metal material mixtures: (A) postdetonation coating, (B) predetonation coating, and (C) premolding/sintering. The axis labels are in normalized weight fraction of the element (or sum of elements) on that axis.

tered and predetonation samples were also treated with 100 μM Fe^{2+} and Fe^{3+} (separately as sulfates in H_2O) to look for possible enhancement of DMPO •OH generation. Selected samples had H_2O_2 added to a final concentration of 2 mM after addition of the buffer and DMPO. DMSO (1 M) and ethanol (1 M) were added to selected samples as •OH scavengers.

Results

Specific-surface area measurements for all hard-metal samples are shown in Table 1**.** Specific surface areas of samples from detonation coating processes were consistently lower than materials from the sintering processes; a few very large clusters (>80 μm) were observed for the postdetonation sample.

Mean particle sizes for the five materials were 2.83, 2.78, 3.22, 3.1, and 3.4 μm for the postdetonation, predetonation, WC, unsintered, and cobalt samples, respectively. Mean particle sizes were on a number, rather than mass basis. SEM results for discrete particle indicated there were numerous particles well below the effective range of the aerodynamic particle sizing instrument, especially for the postdetonation sample. SEM results also included some very large clusters for both the predetonation and postdetonation samples that would be negligible in number but very significant in weight fraction. This may explain the anomalously low specific surface areas for these two types of materials. Most particles from the 5 dust samples were in the respirable size range. Table 2 presents normalized weight percent composition of materials by X-ray fluorescence.

Table 1. Specific Surface Areas (N_2) for Process Materials

sample	BET N_2 (m^2/g) (mean ± SE)
postdetonation	0.115 ± 0.007
predetonation	0.094 ± 0.009
WC	0.66 ± 0.007
unsintered	0.63 ± 0.01
Co	0.56 ± 0

Figure 1 shows the type of discrete particle compositions in terms of W, Co, and other (all other elements past oxygen in the periodic table except W and Co) for postdetonation coating, predetonation coating, and un-

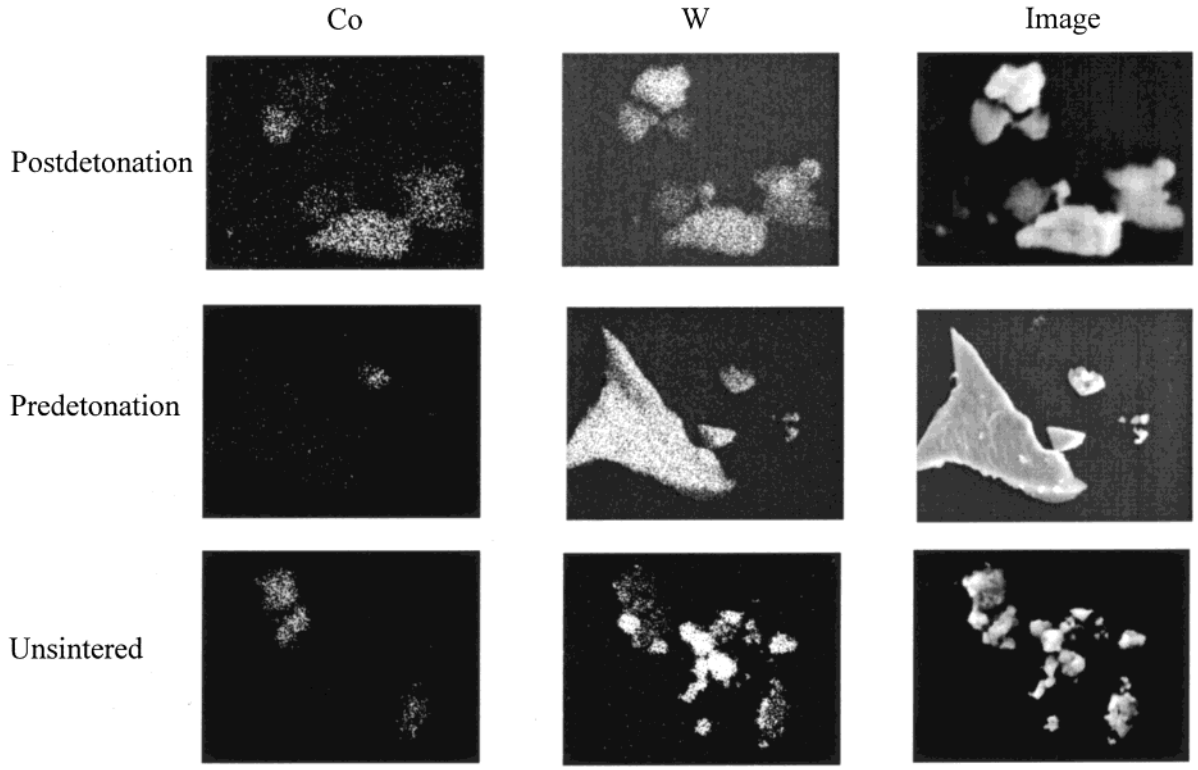

Figure 2. Scanning electron microscopy images, and W and Co elemental maps for hard-metal material mixtures: postdetonation coating, predetonation coating, and premolding/sintering.

Table 2. Chemical Composition of Bulk Samples by X-ray Fluorescence Analysis in (normalized) Weight Percent

element	postdetonation	predetonation	WC	unsintered	Co
W	86.6	87	94	89	<0.006
Co	5.4	6.7	<0.006	5.4	99.85
Fe	0.4	0.50	0.03	0.04	0.04
Cr	1.9	0.06	0.03	0.04	0.01
V	<0.001	<0.001	<0.001	0.05	<0.001
Ni	0.1	0.04	0.02	0.03	0.1
Ti	0.004	0.003	0.001	0.005	0.001
Ta	N/A[a]	N/A	N/A	N/A	<0.006
Nb	0.001	0.001	0.002	0.004	0.001
C	5.6	5.6	6	5.7	0

[a] N/A: could not be quantitated because of spectral interference with other elements.

sintered samples; the other two samples were all WC and Co, respectively. For the postdetonation sample, the "other" category was analyzed, and significant numbers of high-chromium particles were evident (data not shown). Surface contamination by Fe, Co, Cr, and other elements has also been verified for the postdetonation sample in a separate study in progress in this laboratory using scanning Auger spectrometry. The notable difference between the postdetonation coating sample and the other two mixtures is the presence of numerous particles containing elements not present in the predetonation coating material, which shows up in the "other" category. One-quarter of the particles had elements other than W or Co, while the other two samples had fewer than 5% of the particles containing elements besides W and Co.

Particles were also analyzed for inhomogeneous distribution of elements by elemental mapping of discrete particles for W and Co. In Figure 2, the maps for each of these elements, as well as the particle images are shown for pre- and postdetonation coating and unsintered samples; WC and Co samples were homogeneous for all particles examined. The notable difference between the postdetonation materials and the others was the Co contamination of almost all particles. The maps show Co on almost all particles, at least weakly, while Co for the other mixtures tends to be in specific areas as discrete Co particles or in aggregates as Co-rich domains. The Co coverage on the WC and other particles is possible condensation from the vapor phase. The acetylene combustion maximum temperature of 3200 °C is sufficient for vaporization of Co, Fe, Ni, and Cr. Liquid-phase coating from molten metals is also possible.

Selected ESR stacked spectra are shown in Figure 3. The timed measurements of DMPO/•OH adduct formation showed that detonation materials reached a maximum at about 45 min, while the unsintered WC−Co mixture peaked at about 15 min. The average peak areas of three replicate ESR spectra for all five materials are shown in Table 3 for comparison purposes.

All materials except WC showed positive oxygen consumption with time. Oxygen-free treatment of both detonation-coating samples completely eliminated the DMPO/•OH spin adduct signal; the unsintered sample signal intensities of of DMPO/•OH adducts were attenuated almost 21-fold.

The three material mixtures showed sharp signal attenuation with catalase present, extinguishing spectra entirely, indicating that hydrogen peroxide is involved in •OH generation. Addition of H_2O_2 increased DMPO/•OH adducts for both detonation mixtures, but had a negative effect on the signal intensity from the unsintered sample. Superoxide dismutase had a slight negative effect on •OH production by postdetonation materials, a slight positive effect on the predetonation mixture, and almost total extinction of the unsintered mixture ESR signal intensity.

Pre- and postdetonation samples with added sodium formate showed competition with the DMPO spin trap,

Table 3. ESR Spectral Areas (arbitrary units) of DMPO−OH Adducts at 45 min Incubation for Postdetonation and Predetonation Samples, and 15 min for Unsintered Samples, Unless Otherwise Noted

treatment	postdetonation	predetonation	unsintered	WC	Co
$t = 10$ min	101 ± 13.9	31.3 +8.4	32 ± 6.1	12.2 ± 3.3	0
$t = 15$ min	108 ± 15.6	29.0 +5.8	33.4 ± 12.7	16.4 ± 1.2	0
$t = 30$ min	289 ± 12.7	27.2 ± 11.9	29.7 ± 1.3	22.9 ± 5.1	0
$t = 45$ min	405 ± 22.5	45.1 ± 3.2	12 ± 3.4	12 ± 3.2	6.8 ± 1.2
$t = 60$ min	317 ± 8.7	19.2 ± 1.0	19.2 ± 1.0	15.2 ± 5.9	6.0 ± 0.8
− O_2	0	0	1.6		
+ catalase	0	0	0		
+ SOD	392 ± 29.8	60.2 ± 6.1	~3		
+ DETAPAC	131 ± 5.5	0 ± 0	66.6 ± 4.3		
+ deferoxamine	0 ± 0	0 ± 0	24.9 ± 0.8		
+ phenanthroline	18.7 ± 2.5	0 ± 0	23.7 ± 1.1		
+ H_2O_2	614 ± 2.3	67.5 ± 4.1	~0		

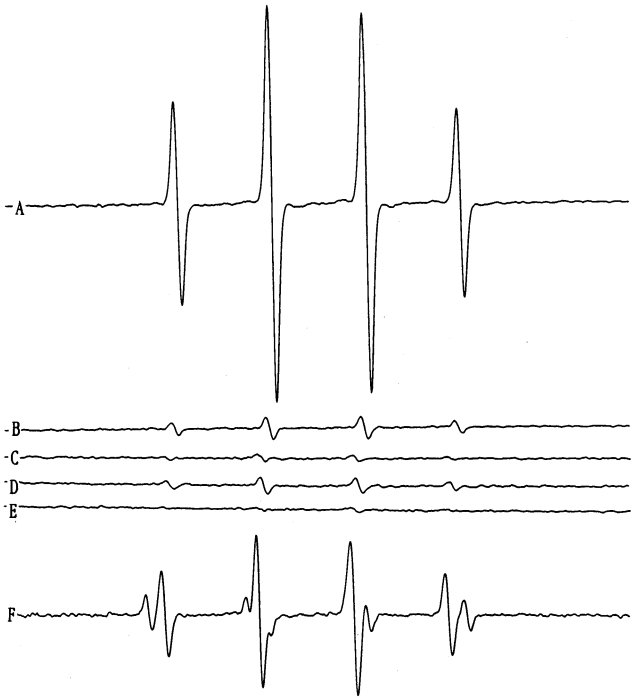

Figure 3. Electron spin resonance spectra recorded after 45 min. of incubation from hard-metal mixtures and ingredients in the presence of 100mM DMPO in pH 7.4 phosphate-buffered saline: (A) postdetonation coating, (B) predetonation coating, (C) WC, (D) premolding/sintering, (E) Co, (F) postdetonation with 50 mM DMPO + 100 mM formate.

and the resultant spectra were weighted sums of the two adduct spectra. The unsintered sample did not show any evidence of formate adducts. DMSO or ethanol did not alter the DMPO/•OH signal intensity for the postdetonation sample, but split the spectra for the predetonation sample, and had no significant effect on the unsintered sample (slight enhancement with no splitting).

Filtered solutions from parallel timed samples showed Co increasing with time for detonation coating and unsintered materials; Fe and Cr were below the detection limits (4 and 0.9 μg, respectively, and Ni was detected from the postdetonation sample at the 15 min (0.1 μg) and 30 min (0.2 μg) points only. Treatment of both detonation-coating materials with three different metal ion chelators strongly attenuated or abolished the spectra. Treatment with deferoxamine did not generate a detectable deferoxamine nitroxide radical spectrum for any of the samples. Conversely, the unsintered sample spectra were strongly enhanced by DETAPAC (more than 2-fold), indicating a markedly different metal ion dependence. Addition of powdered Fe, Cr, and Cr_3C_2 to the unsintered sample resulted in relative attenuations of 5, 22, and 26%, respectively, in the DMPO/•OH signal intensity as compared to unsintered material with no additions. Addition of 100 μM Fe^{2+} to the unsintered and predetonation samples did not increase the DMPO/•OH spectral intensity, while 100 μM Fe^{3+} increased the DMPO/•OH intensity by a factor of 6.8, after 15 min incubation for the unsintered sample, and increased intensity about 22% for the predetonation sample after a 45 min incubation.

Discussion

Hard metal materials were developed in the 1920s, and the first published report of hard-metal lung disease appeared in 1940 (*14*). Progress to clarify the disease mechanism has been difficult. Autopsies of lungs from hard-metal disease victims have shown WC in lungs, but Co content is not present in all the lungs (*15*). In some cases, lungs examined after several months of postexposure showed little or no Co. Co alone has a number of toxic effects, including cardiomyopathy (*16*), asthma, and allergic reactions (*1*), and impaired DNA repair in vitro (*17*−*19*), but most studies have demonstrated that fibrotic lung disease is usually associated with simultaneous exposure to cobalt and other agents (*1*).

Laboratory studies in vivo, using intratracheal Co instillation have shown edema and hemorrhage (*20*), pneumonia, diffuse cellular infiltration, and *bronchiolitis obliterans* (*21*, *22*). When Co was mixed with WC in powdered form and instilled, transient inflammation was followed by fibrosis in the areas of retained particles (*21*). Several additional studies showed that pulmonary fibrosis follows instillation of hard-metal materials (*23*−*25*), and toxicity and cobalt bioavailability were much greater for the Co−WC mixture than either Co or WC alone (*25*).

In vitro study results are similar in that hard-metal mixtures are highly effective at inducing cellular toxicity, while WC is generally inert and Co is less toxic. Other transition metals can be substituted for WC with comparable results, but other "inert" particles are not effective, demonstrating that toxicity is not due to a carrier particle effect (*26*). Soluble cobalt is also not the sole cytotoxic component of hard-metal mixtures in vitro, and is less toxic than the hard-metal WC−Co mixture (*27*).

A mechanism that has been suggested for a number of agents associated with pulmonary fibrosis is the generation of reactive oxygen species (ROS). Recent studies (*28*) have demonstrated that hard-metal presintering mixtures are potent generators of ROS, such as

•OH radicals, while the component WC and Co materials are inert or only very weak producers of these oxygen species. Additionally, antioxidants such as butylated hydroxytoluene sharply reduce macrophage damage induced by hard-metal materials in vitro (*28*, *29*). The ROS mechanism is notably consistent with observations that the component WC and Co materials are less toxic than the hard-metal WC−Co mixture in both in vitro and in vivo studies. It should be noted here that although WC is not considered toxic or a ROS generator itself, it has potent catalytic properties that allow replacement of Pt in many applications (*30*) and may function to facilitate oxygen reduction in hard-metal-induced ROS generation.

The results obtained in the present study confirm that •OH radicals are generated by hard-metal materials and extend the findings of Lison et al. (*28*) to new, related materials, detonation coating materials. The unsintered materials used in this study were apparent producers of DMPO/•OH adducts, but further study indicated that they were probable degradation products of DMPO/•O_2^- adducts. This is supported by the observations that DMPO/•OH adducts were (a) almost eliminated by SOD, (b) not competitively scavenged with formate ions, and (c) not scavenged by DMSO or ethanol, with resultant split adduct spectra with DMPO. Results are consistent with reaction 2, which generates Co^{2+} as well as hydrogen peroxide; UV−vis spectrophotometry was used to confirm the presence of Co^{2+} in this system; Co^{2+} increases with time for the unsintered and both detonation materials (data not shown).

$$Co + O_2 + 2H^+ \rightarrow Co^{2+} + H_2O_2 \text{ (possibly site-specific)} \quad (2)$$

Co^{2+} reaction with H_2O_2 does not produce •OH directly (*32*), but has been shown to generate •O_2^-, which can be trapped by DMPO. The DMPO/•O_2− adduct is known to decompose yielding the DMPO/•OH adduct (*31*).

The dramatic enhancement of •OH formation after treatment with DETAPAC suggests Co^{3+} involvement. Normally, the 1.8 V $E°$ for oxidation of Co^{2+} makes the oxidation very difficult, but proper ligands in chelators such as EDTA, DETAPAC, etc. can lower the $E°$ to ∼0.2 V, and allow generation of •OH (*33*).

$$Co^{2+}\text{−EDTA } H_2O_2 \rightarrow Co^{3+}\text{−EDTA} + OH^- + {}^\bullet OH \quad (3)$$

Addition of Fe, Cr, and Cr_3C_2 did not increase •OH formation to that of the postdetonation material, despite the same elemental composition, suggesting that other properties, such as elemental distribution or other elements of the postdetonation material are important for the enhanced •OH generation. The fact that adducts decreased after addition of the metals and metal carbide may be due to adsorption or consumption of O_2 by the added materials. Addition of Fe^{3+} to H_2O suspensions of the unsintered material strongly increased DMPO/•OH formation; this is consistent with the suggestion of Eberhardt et al.(*33*) of Fe^{3+}-assisted oxidation of Co^{2+}.

The predetonation sample, although quantitatively similar to unsintered material in •OH generation, showed different chemical behavior. Catalase also extinguished the •OH ESR signal, but SOD had little effect, and chelators strongly reduced the signal intensity. This suggests other metal ions, such as Fe, may be important in oxygen reduction in this system. While reaction 2 would be unchanged, Fenton chemistry with Fe, present at 0.5%, is probably also important; Fe^{2+} can be regenerated, and need be present only at micromolar concentrations to permit •OH generation (*33*):

$$Fe^{2+} + H_2O_2 \rightarrow Fe^{3+} + OH^- + {}^\bullet OH \quad (4)$$

$$Fe^{3+} + O_2^- \rightarrow Fe^{2+} + O_2 \quad (5)$$

Addition of 100 μM Fe^{3+} increased •OH adducts about 22%. The selective Fe chelators deferoxamine and 1,10-phenanthroline, would inhibit both reactions 4 and 5 as observed, and chelation of Fe with EDTA, similar to DETAPAC, has been observed to slow •OH generation by Fenton chemistry when both Co and Fe ions are present (*33*). Addition of DMSO and ethanol as •OH scavengers resulted in split spectra consistent with DMPO adducts of •CH_3 and •$CH(OH)CH_3$, respectively, indicating release of •OH in solution. Deferoxamine also functions as an •OH scavenger, but the distinctive deferoxamine-DMPO/•OH spectrum was not observed in this study.

The postdetonation sample was a much stronger generator of DMPO/•OH adducts than the other two mixtures, but was very similar to the predetonation sample in terms of the effect of chelators, again suggesting the involvement of Fe in •OH generation. Elemental distribution was strikingly different from the presintered sample, with a very close homology of Co and WC maps, consistent with deposition of liquid or vapor-phase Co on many WC particles. Surface analysis using Auger electron spectroscopy, currently in progress, indicates a substantial fraction of particles contain surface-layer Fe, as well as Co, with lesser amounts of Cr and Ni. For example, in a typical field of 31 postdetonation particles, 21 contained substantial Fe, with several having Fe as the principal surface element.

Catalase extinguished the •OH ESR signal as it did for the other samples, and SOD exhibited a minor inhibitory effect. The addition of •OH scavengers DMSO and ethanol had no observable effect on the DMPO/•OH signal intensity, indicating site-specific formation of the DMPO/•OH adducts.

Overall, detonation-coating materials are altered substantially in the coating process, and show features and compositions that are different from both the feedstock material and materials from sintering processes. The surface contamination, as well as formation of clusters with process debris from other coating operations, produces a situation favorable for ROS production: WC adsorption could provide a high local O_2 concentration on the WC surface, in close proximity to reducing agents, such as Fe and Co, either on surfaces or adjacent particles.

Ongoing studies in this laboratory also indicate enhanced induction of micronuclei in V 79 cells in vitro, relative to the other hard-metal materials of this study (data not shown, manuscript in preparation). Since the lifetime of •OH is very short in solution (∼1×10^{-10} s), it must be produced in close proximity to vulnerable molecules or structures to exhibit damaging effects of this radical. Direct particle or fiber interactions with chromosomes has been observed for chrysotile asbestos fibers (*34*), and •OH damage of DNA is well established (e.g.,

bleomycin) (*35*). While ROS/•OH has not been proven to cause hard-metal disease or other types of fibrotic lung disease, it is consistent with mechanistic studies of other fibrogenic agents, such as bleomycin (*35*).

In conclusion, the postdetonation particles studied have a distinctive morphology and composition, and these properties are highly favorable for the production of reduced oxygen species. Further study is needed to verify these findings in vitro and in vivo and to examine materials and airborne dusts from similar processes, such as plasma and high velocity oxy-fuel coating technologies.

Acknowledgment. The authors would like to thank Mr. Stephen Leonard for valuable assistance with electron spin resonance spectroscopy and Dr. Xianglin Shi for many valuable discussions and suggestions.

References

(1) Lison, D. (1996) Human Toxicity of cobalt-containing dust and experimental studies on the mechanism of interstitial lung disease (hard metal disease). *Crit. Rev. Toxicol.* **26**, 585−616.
(2) NIOSH (1977) *Criteria for a recommended standard: Occupational exposure to tungsten and cemented tungsten carbide*, DHEW (NIOSH) Publication 77−127, NTIS PB-275594, Cincinnati, OH.
(3) Shirakawa, T., Kusaka, Y., Fujimura, N., Goto, S., Kato, M., and Heki, S. (1989) Occupational asthma from cobalt sensitivity in workers exposed to hard metal dust. *Chest* **95**, 29−37.
(4) Kusaka, Y. (1983) Hard metal asthma: a case of allergic bronchial asthma and contact dermatitis due to metallic cobalt. *Nippon Kyubu Shikkon Gakkai Zasshi* **21**, 582−586.
(5) Davison, A., Haslam, P., Corrin, B., Coutts, I. I., Dewar, A., Riding, W., Studdy, P., and Newman-Taylor, A. (1983) Interstitial lung disease and asthma in hard-metal workers: bronchioalveolar lavage, ultrastructural, and analytical findings and results of bronchial provocation tests. *Thorax* **38**, 119−128.
(6) Kusaka, Y., Ichikawa, Y., Shirakawa, T., and Goto, S. (1986) Effects of hard metal dust on ventilatory function. *Br. J. Ind. Med.* **43**, 486-489.
(7) Moulin, J., Wild, P., Romazini, S., Lasfargues, G., Peltier, A., Bozek, C., Deguerry, P., Pellet, F., and Perdrix, A. (1998). Lung cancer risk in hard-metal workers. *Am. J. Epidemiol.* **148**, 241−248.
(8) Auchincloss, J., Abraham, J., Gilbert, R., Lax, M., Henneberger, P., Heitzman, E., and Peppi, D. (1992) Health hazard of poorly regulated exposure during manufacture of cemented tungsten carbides and cobalt. *Br. J. Ind. Med.* **49**, 832−36.
(9) Fischbein, A., Luo, J.-C., Solomon, S., Horowitz, S., Hailoo, W., and Miller, A. (1992) Clinical findings among hard metal workers. *Br. J. Ind. Med.* **49**, 17−24.
(10) Sluis-Cremer, G., Glyn Thomas, R., and Solomon, A. (1987) Hard-metal lung disease. A report of 4 cases. *S. Afr. Med. J.* **71**, 598−600.
(11) IARC (1991) *IARC monographs on the evaluation of carcinogenic risks to humans*, Vol. 52. IARC, Lyon, France.
(12) Beckett, W., Figuerola, S., Gerstenhaber, B., Welch, L., Klimstra, D., and Smith, G. J. W. (1992) Pulmonary fibrosis associated with occupational exposure to hard metal at a metal-coating plant. *Morbidity Mortality Weekly Rep.* **41** (4), 65−67.
(13) Figuerola, S., Gerstenhaber, B., Welch, L., Klimstra, D., Smith, G. J. W., and Beckett, W. (1992) Hard metal interstitial pulmonary disease associated with a form of welding in a metal parts coating plant. *Am. J. Ind. Med.* **21**, 363−373.
(14) Jobs, H., and Ballhausen, C. (1940) Powder mettalurgy as a source of dust from the medical and technical standpoint. *Vertrauenarzt Krankkasse* **5**, 142−148.
(15) Stettler, L., Groth, D., and Platek, S. (1983) Automated Characterization of particles extracted from human lungs: Three cases of tungsten carbide exposure. *Scanning Electron Microsc.* **1983**, 439−448.
(16) Alexander, C. (1972) Cobalt-beer myopathy. A clinical and pathologic study of twenty-eight cases. *Am. J. Med.* **53**, 395−417.
(17) Beyersmannn, D. (1994) Interactions in metal carcinogenicity. *Toxicol. Lett.* **72**, 1−3.
(18) Leitao, A., Soares, R., Cordoso, J., Guillobel, H., and Caldas, L. (1993) Inhibition and induction of SOS responses in *Escherichi coli* by cobaltous chloride. *Mutat. Res.* **286**, 173−180.
(19) Hartwig, A., Snyder, R., Schepegrell, R., and Beyersmann, D. (1991) Modulation by Co(II) of UV-induced DNA repair, mutagenesis and sister chromatid exchanges in mammalian cells. *Mutat. Res.* **248**, 177−185.
(20) Harding, H. (1950) Notes on the toxicology of cobalt metal. *Br. J. Ind. Med.* **7**, 76−78.
(21) Schepers, G. (1955) The biological action of tungsten carbide and cobalt. *Arch. Ind. Health* **12**, 140−146.
(22) Delahant, A. (1955) Experimental study of the effects of rare metals on animal lungs. *Arch. Ind. Health* **12**, 116−120.
(23) Kitamura, H., Yoshimura, Y., Tozawa, T., and Koshi, K. (1980) Effects of cemented tungsten carbide dust on rat lungs following intratracheal injection of saline suspension. *Acta Pathol. Jpn.* **30**, 241−253.
(24) Lasfargues, G., Lison, K., Maldague, P., and Laurwerys, R. (1992) Comparative study of the acute lung toxicity of pure cobalt powder and cobalt−tungsten carbide mixture in rat. *Toxicol. Appl. Pharm.* **112**, 41−50.
(25) Lasfargues, G., Lardot, C., Delos, M., Laurwerys, R., and Lison, D. (1995) The delayed lung responses to single and repeated intratracheal administration of pure cobalt and hard metal powder in the rat. *Environ. Res.* **69**, 108−121.
(26) Lison, D., and Lauwerys, R. (1995) The interaction of cobalt metal with different carbides and other mineral particles on mouse peritoneal macrophages. *Toxicol. in Vitro* **9**, 341−347.
(27) Lison, D., and Laurwerys, R. (1992) Study of the mechanism responsible for the elective toxicity of tungsten carbide powder toward macrophages. *Toxicol. Lett.* **60**, 203−210.
(28) Lison, D., Carbonnelle, P., Mollo, L., Lauwerys, R., and Fubini, B. (1995) Physicochemical mechanism of the interaction between cobalt metal and carbide particles to generate toxic activated oxygen species. *Chem. Res. Toxicol.* **8**, 600−606.
(29) Lison, D., and Laurwerys, R. (1993) Evaluation of the role of reactive oxygen species on the interactive toxicity of carbide-cobalt mixtures on macrophages in culture. *Arch. Toxicol.* **67**, 347−351.
(30) Bennett, L., Cuthill, J., McAlister, A., and Erickson, N. (1974) Electronic structure and catalytic behavior of tungsten carbide. *Science* **184**, 563−565.
(31) Pou, S., Hassett, D. T., Britigan, B. E., Cohen, M. S., and Rosen, G. M. (1989). Problems associated with spin trapping oxygen-centered free radicals in biological systems. *Anal. Biochem.* **177**, 1−6.
(32) Hanna, P., Kadiiska, M., and Mason, R. (1992) Oxygen-derived free radical and active oxygen complex formation from cobalt-(III) chelates in vitro. *Chem. Res. Toxicol.* **5**, 109−115.
(33) Eberhardt, M., Santos, C., and Soto, M. (1993) Formation of hydroxyl radicals and Co^{3+} in the reaction of Co^{2+}-EDTA with hydrogen peroxide. Catalytic effect of Fe^{3+}. *Biochim. Biophys. Acta* **1157**, 102−106.
(34) Wang, N., Jaurand, M. C., Magne, L., Kheuang, L., Pinchon, M. C., and Bignon, J. (1987) The interaction between asbestos fibers and metaphase chromosomes of rat pleural mesothelial cells in culture. *Am. J. Pathol.* **126**, 343−349.
(35) Povirk, L. F., and Austin, M. J. F. (1991) Genotoxicity of bleomycin. *Mutat. Res.* **257**, 127−143.

TX0100688